

Modelling of the Venusian Lithosphere

Lorenz Veithen (5075211) - Hours spent: 30h

July 6, 2023

1 Introduction

A deep comprehension of the formation processes of the surface of rocky planets provides clues about its tectonic evolution and current state. In turn, those aspects are fundamental in the quest to grasp the origin of life and the formation of the planetary systems. From the young surface of Triton to the fascinating landscapes of Mars and the volcanoes of Venus, planetary surfaces have the potential to yield crucial insights into the internal structure of the body. In this paper, numerical models for variations in the crustal thickness of Venus are developed and compared to literature.

Venus has been studied in great details through observational studies, and a range of space missions. These yielded the information provided in Table 1, and topography and gravity data, which will be used to build and verify the models in this study. Additionally, a wide variety of layered models of Venus have been investigated, such as the four-layer model proposed by Aitta [1] and repeated in Table 2, which is used as reference in this study. Furthermore, although the majority of missions focused on the Venusian atmosphere, two carried experiments targeting the interior of the planet. Namely, Venus Express studied the magnetic field of the planet [2] and yielded data on its surface temperature [3], and Magellan permitted to obtain gravity field and topography data of the planet [4]. The latter two are the main inputs for the development of the models in this research, as explained in the following section.

Table 1: Observational data and parameters of Venus.

| Parameters | Values |
|--|------------|
| Mass, M , [5, 6], [kg] | $4.869E24$ |
| Equatorial radius, R_{eq} , [5, 6], [km] | 6051.53 |
| Mean density, $\bar{\rho}$, [5, 6], [kg/m^3] | 5250 |
| Gravitational parameter, μ , [7], [km^3/s^2] | 324858.6 |

Table 2: Four layer model used by [8]. M=Mantle, L=Lower, U=Upper.

| Layers | Core | L-M | U-M | Crust |
|-----------------------------------|------|------|------|-------|
| r [km] | 3228 | 5332 | 6022 | 6052 |
| ρ [kg/m^3] | 9800 | 4850 | 3760 | 2900 |

A number of studies considered the lithosphere of Venus and aimed to determine the thickness and density distributions of the crust of the planet.

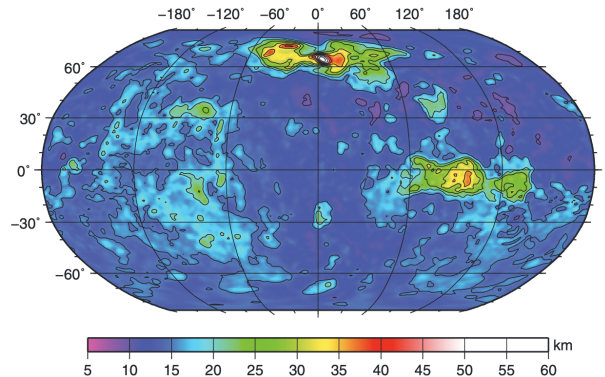


Figure 1: Spatial distribution of the crustal thickness from [13], for a mean crustal thickness of 15km, and a mantle load depth of 250km.

Particularly, the correlation between the gravity and topography of planets has been the primary tool to determine the lithospheric parameters, including its elastic and crustal thicknesses [9, 10, 11]. According to Anderson and Smrekar [12], two related parameters are sensitive to these parameters: the admittance (how much gravity anomaly is created by a unit of topography) and coherence (measure of similarity between the two signals). While coherence would generally provide more robust results than admittance, the latter is currently used due to the low resolution of the gravity data [12]. Therefore, Anderson and Smrekar [12], used predicted and observed global admittance maps of the Venusian lithosphere to invert its elastic, crustal, and lithospheric thicknesses. They found that about half of the planet has $T_e < 20\text{km}$ (elastic thickness, hence the flexural response cannot be distinguished from isostasy), the lithospheric properties vary on scales of 1000km, and crustal thicknesses vary from 10 to 70 km [12].

Another approach was taken by Wei, Yang, and Huang [13], who inverted the mass anomalies at two different depths, permitting to solve for the crustal thickness and a spatial map of the mantle mass anomalies. This approach permits to separate the shallow and deep compensation mechanism, contributing to the observations. As a result, mean thicknesses of the crust in the range of 8-25km were obtained, with typical variations of the crust-mantle boundary depth as shown in Fig. 1.

Contrary to the results shown by Anderson and Smrekar [12], according to James, Zuber, and Phillips [14], the gravity and topography of Venus are strongly influenced by its internal dynamical processes. This hints that the description of the Venusian lithosphere through isostasy-based models will yield large gravity

residuals, it is necessary to take into account dynamical effects on gravity and topography to accurately determine the crustal thickness of the planet. Therefore, James, Zuber, and Phillips [14] first identified the relationship between the gravity and topography for the convection model developed by Huang, Yang, and Zhong [15], and used a dynamical admittance model to compute the crustal thickness of the planet using the spherical formula from [16]. As a result, the study obtained maps of the crustal thickness with and without dynamical effects, as shown in Figure 2.

In this assignment, the crustal thickness and lateral density variations of Venus are determined through three different types of models of increasingly physical nature: Bouguer inversion, Airy isostasy, and flexural isostasy. The residuals of each model in describing the gravity fluctuations are analysed and compared to each other. Following, the elastic thickness parameter of the planet is estimated by fitting the flexural isostasy model to the observed gravity field. The resulting flexural isostasy model is used to invert lateral density variations in the crust.

The paper is structured in the following manner. section 2 describes the methodologies used for each of the three aforementioned models. Then, section 3 presents the key results obtained from the application of the models, including heat maps of crustal thickness and densities and gravity residuals. Those results are analysed and discussed with respect to literature in section 4, and the validity of the approach is briefly reflected upon in section 5. Finally, conclusions and recommendations on further work in the field are given in section 6.

2 Methodology

2.1 Data Acquisition

The topographic and gravity data were retrieved from [17] to perform this study. The former has a 1×1 degree resolution of the Venusian topography, and is a 360×180 grid from -89.5 to 89.5 degrees latitude, and 240 to 240 degrees longitude, increasing from west to east. Furthermore, it was derived from Ford and Pettengill [18], Magellan topography data completed with Pioneer Venus Orbiter topography data. The gravity data takes the form of the spherical harmonic coefficients, determined from radio tracking and the Magellan mission data [17]. However, the power spectrum of the gravitational potential is smaller than the error for Degree and Orders (D/O) higher than (60, 60), as shown by Figure 3. Therefore, only coefficients up to D/O (60, 60) are used throughout the study.

The data is processed using the GSH software [19] in MATLAB.

2.2 Data Processing

The topographic and gravity data are plotted in Figure 4. For a regular flattened body, following the (flattened) onion-shell model, only the C_{00} and C_{20} spherical harmonics coefficients are non-zero, and any deviation from that gravity field can be linked to either the topography or the internal structure of the planet. Using knowledge of the surface topography from Figure 4a and Eq. (1) (the Bouguer correction which models the impact of the topography on the gravity field), Eq. (2) permits to single-out the planetary interior contribution to the gravity field deviations.

$$\delta g_{topo} = 2\pi G h \rho_{crust} \quad (1)$$

$$g_B = g_{obs} - \delta g_{topo} \quad (2)$$

where $G = 6.6743E-11$ is the universal gravitational constant, h is the height of the topography at the position, ρ_{crust} is the density of the crust (density of surface features), and g_{obs} is the observed gravity field (with $C_{00} = C_{20} = 0$). This residual is the Bouguer anomaly, and directly reflects the interior structure, with the major component being the fluctuations in the thickness of the crust.

2.3 Numerical Models

A number of numerical models are developed and compared (or fitted) to the observed gravity field (with $C_{00} = C_{20} = 0$), with the goal of gaining insights into the crustal thickness and density variations on the planet. The GSH software is used to determine the spherical harmonic gravity field arising from a given lithosphere model, which is then compared to the observed gravity field (removing C_{00} and C_{20}). Each numerical method aims to adapt the depth of the crust-mantle boundary of a reference model of the lithosphere, each with a different approach. Following, the resulting crustal thickness flexural model which best fits the observed gravity field will be selected to determine the lateral density variations over the planetary crust. The reference model is divided into two layers: from topography altitude to $D = -30$ km (crustal density) and from D to -200km depth (mantle density). This value of D is taken from [1]. The crust and mantle densities (ρ_c and ρ_m) are kept constant in all numerical models, and determined from results of the Bouguer inversion model for different combinations of ρ_c and ρ_m .

2.3.1 Bouguer Inversion Model

The Bouguer inversion makes use of the observed data directly to fit the crustal thickness using the iterative inversion shown in Figure 5. In this scheme, $r_{ref} = D$ given by the reference model, and a tolerance of 1E-4 was used. It must be noted, however, that this type of method will result in an overfitting of the observed gravity field, and therefore needs to be considered with care. This model gives rise to an uncompensated topography (zero isostasy) [20], with variations in crustal thickness which cannot always be explained through a physics model of the crust.

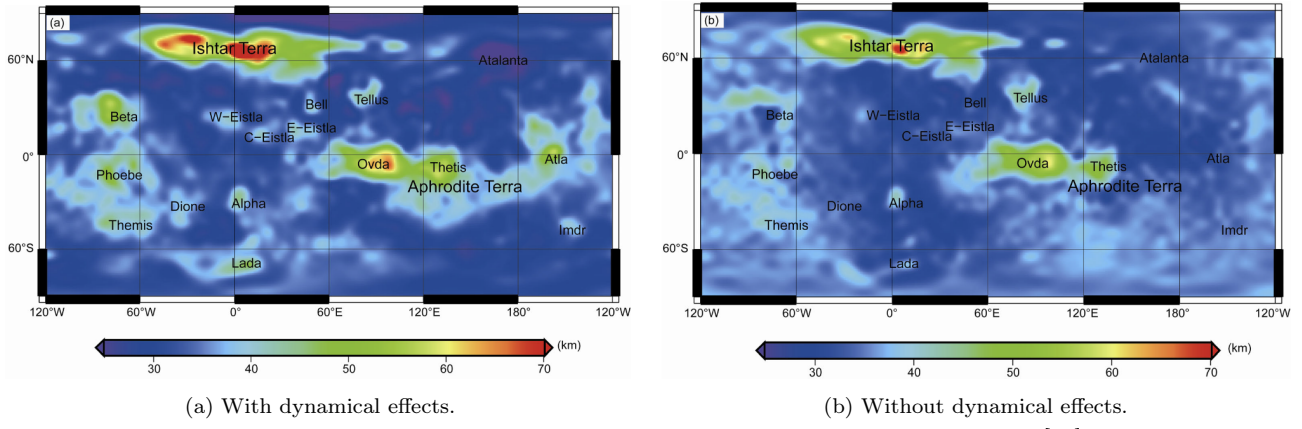


Figure 2: Crustal thickness of Venus according to James, Zuber, and Phillips [14].

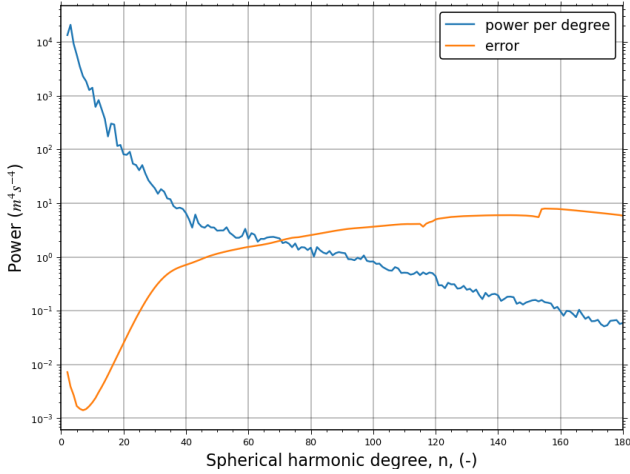


Figure 3: Power spectrum of the Venus spherical harmonic gravity field, from [17].

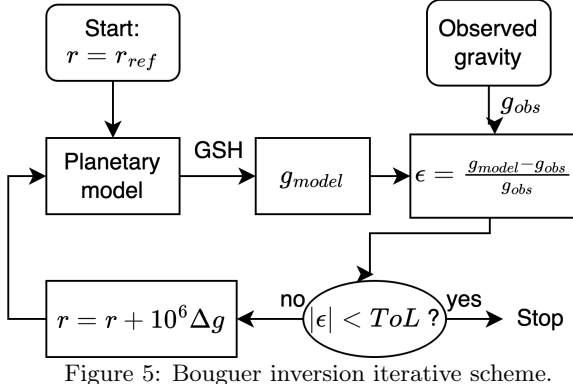


Figure 5: Bouguer inversion iterative scheme.

2.3.2 Airy-Heiskanen Model

The Airy-Heiskanen [21] model is a simple, 1D, local isostasy model to determine the depth of the crust-mantle boundary due to the topography, using Eq. (3). This correction is applied to the reference crustal thickness, D , using Eq. (4).

$$\Delta r = \frac{h\rho_c}{\rho_m - \rho_c} \quad (3)$$

$$r = D - \Delta r \quad (4)$$

This model implies that a higher topography implies a larger thickness of the crust beneath it, as D

is defined negative and Δr is more positive for higher surface features.

2.3.3 Flexural Isostasy Model

An infinite plate flexure model of the crust permits to obtain a more realistic description of the lithosphere response to the topography, as the level of isostasy is determined by the scale of the surface feature. The flexural response surface is computed based on the Δr obtained from Eq. (3). First, Δr is converted to the spectral domain by determining \bar{A}_{nm} and \bar{B}_{nm} ,

$$\Delta r(r, \theta, \phi) = \sum_{n=0}^{\infty} \sum_{m=0}^n \left(\frac{R}{r} \right)^n \left[\bar{A}_{nm} \cos(m\phi) + \bar{B}_{nm} \sin(m\phi) \right] P_{nm}(\cos \theta) \quad (5)$$

Following, the spherical harmonic coefficients of Δr are multiplied by the infinite plate flexural response function Eq. (7), where the D is the flexural rigidity given by Eq. (6),

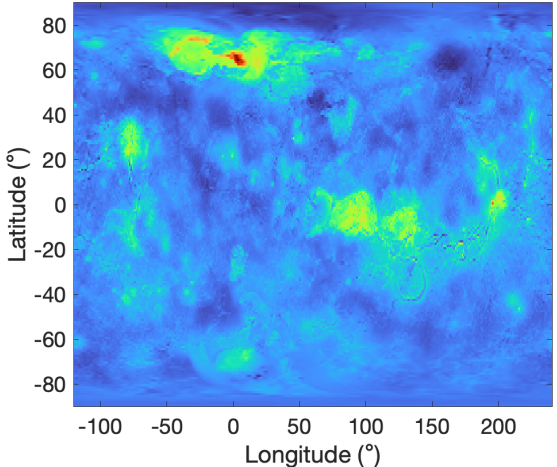
$$D = \frac{ET_e^3}{12(1-\sigma^2)} \quad (6)$$

$$\Phi(n) = \left(1 + \frac{D}{(\rho_m - \rho_c)g} \left(\frac{2(n+1)}{2R} \right)^4 \right)^{-1} \quad (7)$$

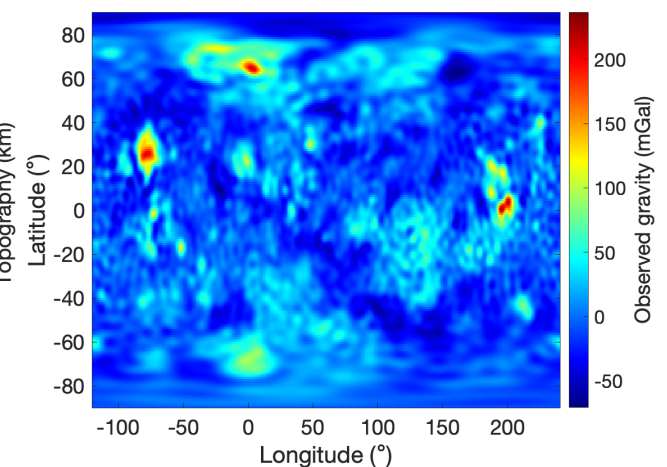
where n is the spherical harmonic degree, R is the reference radius of the field, $g = 8.87 \text{ m/s/s}$ is the gravity (taken as surface gravity [5]), $E = 90 \text{ GPa}$ is the elastic modulus of the crust [22], $\sigma = 0.23$ is the Poisson ratio of the crust [23], and T_e is the effective elastic thickness of the planet. Such that,

$$\begin{bmatrix} \bar{A}_{nm}^{flexure} \\ \bar{B}_{nm}^{flexure} \end{bmatrix} = \Phi(n) \begin{bmatrix} \bar{A}_{nm} \\ \bar{B}_{nm} \end{bmatrix} \quad (8)$$

The coefficients are then assembled in the spherical harmonic function as,



(a) Topography



(b) Z-component of the gravitational force at zero altitude.

Figure 4: Gravity and topography maps of Venus from [17]. Note that the maps are centred around the 120° longitude (60° E), to allow for a better visualisation.

$$\Delta r^{flex}(r, \theta, \phi) = \sum_{n=0}^{\infty} \sum_{m=0}^n \left(\frac{R}{r}\right)^n \left[\bar{A}_{nm}^{flexure} \cos(m\phi) + \bar{B}_{nm}^{flexure} \sin(m\phi) \right] P_{nm}(\cos \theta) \quad (9)$$

and Eq. (4) is used to compute the new crust-mantle boundary depth. Although the elastic thickness parameter depends on the position on the planet surface, the model is simplified through the consideration of a single value at $T_e = 22$ km based on [24], who found values ranging from 19 and 29 km with a mean value around 21-23km. Additionally, an optimal value of the T_e parameter is obtained by fitting the modelled to the observed degree variance (see below). The fit is performed using the *fmincon* MATLAB method in the bounds $0 < T_e < 1000$ km, to reduce the residual formulated as (DV is the degree variance vector),

$$\epsilon = \sqrt{\sum_i \left(\frac{DV_{obs} - DV_{model}}{DV_{obs}} \right)_i^2} \quad (10)$$

which permits to treat all degrees with equal importance, as all the differences are expressed as percentages.

2.3.4 Density Inversion

With the crustal thickness obtained from the flexural isostasy model using an optimal value of the elastic thickness T_e , the lateral density variations in the crust are inverted. The inversion is performed similarly to the Bouguer inversion, with the only difference being that the scaling factor of the gravity residual is $1E4$ instead of $1E6$ in Fig. 5. Those lateral density variations can then be compared to a geological map of Venus.

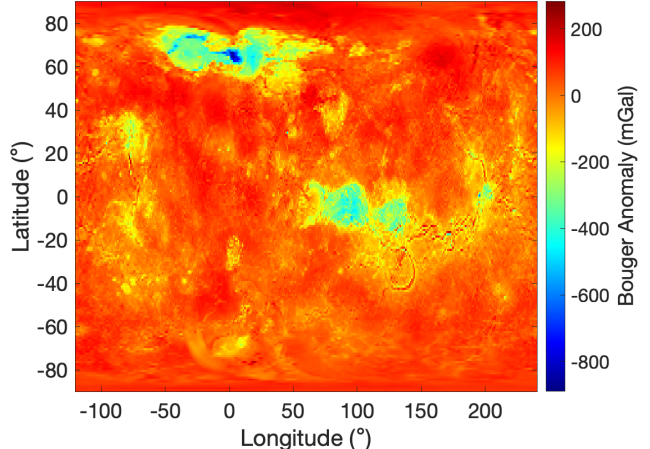


Figure 6: Bouguer anomaly.

2.4 Data Analysis and Representation

Two main types of plots are used to show the variations in crustal thickness and densities across the planet. First, heat maps showing the parameter variation as a function of the longitude and latitude, with a resolution of 1×1 degree, which is limited by the topographic data available. Second, the degree variance of the spherical harmonic gravity field is computed and plotted as a function of the coefficient degree, based on Eq. (11),

$$\sum_{m=0}^n (C_{nm}^2 + S_{nm}^2) \quad (11)$$

where (n, m) is the degree-order.

3 Results

First, Fig. 6 shows the Bouguer anomaly obtained from Eq. (2) (with $\rho_c = 2900$ kg from Tab. 2), which clearly indicates that the higher order spherical harmonics coefficients of the gravity field cannot be completely explained by the topography. This reveals that variations in the crustal thickness and density exist.

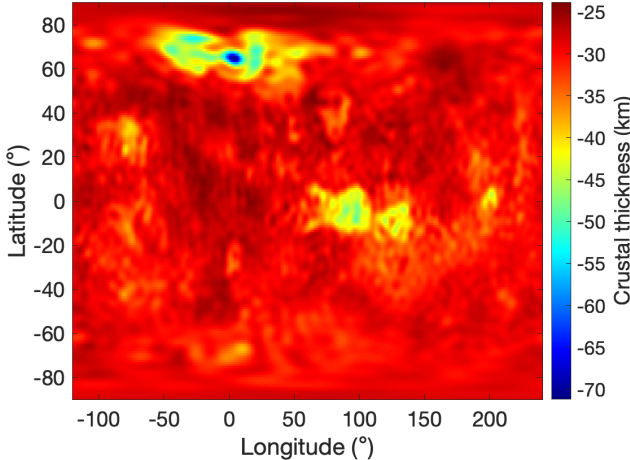


Figure 7: Crustal thickness based on the Bouguer inversion.

Following, the Bouguer inversion numerical model was run with different combinations of crust and mantle densities, as shown in Tab. 3. The combinations were chosen based on Aitta [1] and James, Zuber, and Phillips [25]. Combination number four is found to come the closest to the ranges shown in recent literature (Fig. 2, [14]), and will be used for the subsequent analysis (the Bouguer anomaly analysis was not repeated as the same conclusions would be drawn). The crustal thickness obtained with the Bouguer inversion and those densities is shown in Fig. 7 (note that residuals can be made arbitrarily small with this model and are therefore omitted).

The crustal thickness obtained using the two remaining numerical models (with $\rho_c = 2700\text{kg/m}^3$ and $\rho_c = 3300\text{kg/m}^3$) are given in Figs. 8, and 9, with their associated gravity residuals. Additionally, the crustal thickness variations along the 0.5° latitude line for each of the three models and the associated topography are shown Fig. 10a.

Table 3: Effect of different combinations of crust and mantle densities on the Bouguer inversion. The densities are given in kg/m^3 ; the minimum, mean, maximum and standard deviation (STD) are given in km.

| | ρ_c | ρ_m | min | mean | max | STD |
|---|----------|----------|---------|--------|--------|------|
| 1 | 2900 | 3300 | -102.09 | -29.89 | -19.92 | 5.87 |
| 2 | 2900 | 3760 | -60.63 | -29.95 | -25.29 | 2.70 |
| 3 | 2900 | 4500 | -45.92 | -29.97 | -27.46 | 1.45 |
| 4 | 2700 | 3300 | -71.14 | -29.93 | -23.90 | 3.56 |
| 5 | 2700 | 3760 | -52.33 | -29.96 | -26.54 | 2.01 |
| 6 | 2700 | 4500 | -42.87 | -29.98 | -27.96 | 1.18 |

The degree variance of the spherical harmonic gravity fields obtained from the three numerical models, and the observation data, are shown in Fig. 10b. The mismatch between the flexural model and the observation data degree variance was reduced through optimisation of the T_e parameter for the residual from Eq. (10). It was then found that $T_e = 31.454\text{km}$ provides the best fit of the flexural model to the observed degree variance.

This optimal fitting flexural isostasy model was used to invert the crustal lateral density variations, Fig. 11a.

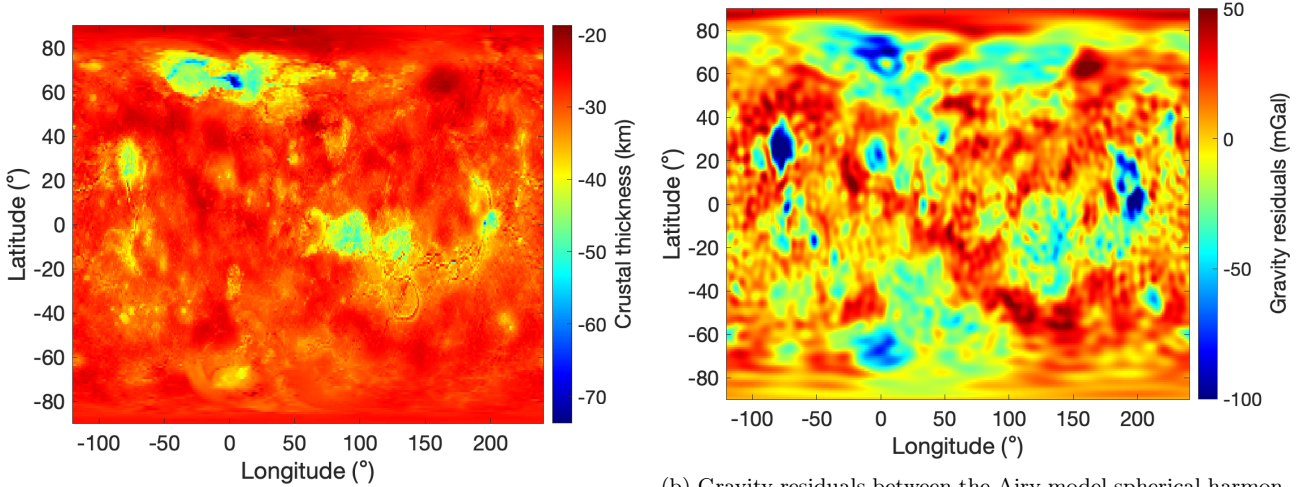
4 Discussion

The Venusian Bouguer anomaly shown in Fig. 6 demonstrates that the gravity field fluctuations cannot be solely attributed to the surface topography, and that models of the spatial distribution of the crustal thickness and density are necessary. The results obtained match the statistics and maps provided by [29].

Considering the effect of the crust and mantle densities on the Bouguer inversion, a few observations can be made based on Tab. 3: (1) the mean crustal thickness consistently stays around $D = -30\text{km}$; (2) while a lower mantle density results in a (slightly) thinner crust on average, the minimum and maximum values become further apart and a larger spread of the data is found; (3) changes in the crustal density has a larger impact for a larger mantle densities. Furthermore, as already noted in the previous section, the combination $\rho_c = 2700\text{kg/m}^3$ and $\rho_c = 3300\text{kg/m}^3$ fits the results of [14] the best and was chosen for subsequent models.

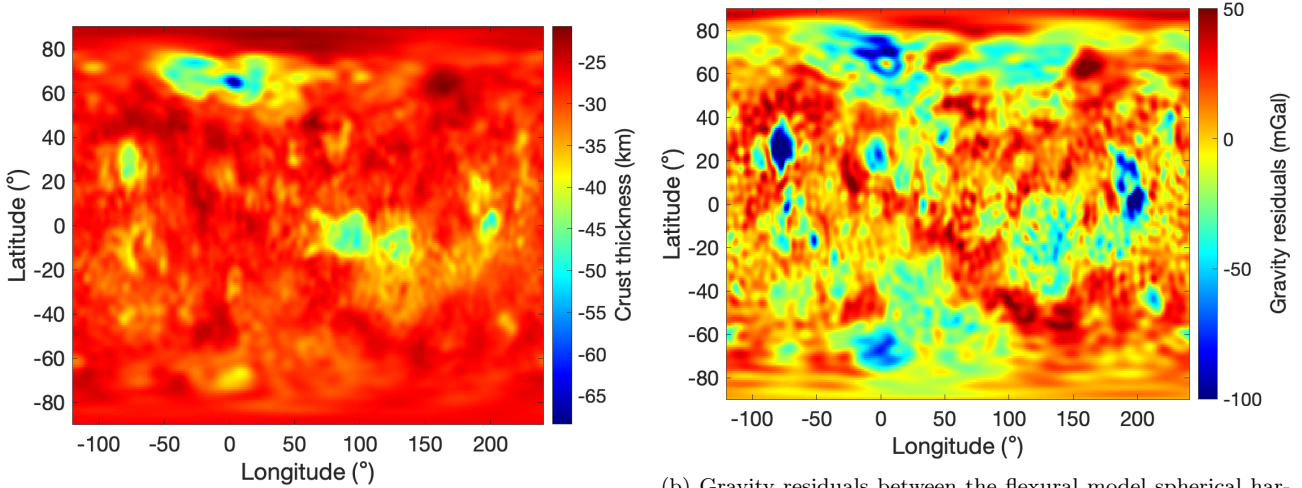
Considering Figs. 8b and 9b, it is apparent that the residuals between the observed and modelled gravity field for both the Flexural and Airy models are very similar. This is a result of the low elastic thickness used ($T_e = 22\text{km}$), making most of the flexural isostasy local, like the Airy model. This is further confirmed by Fig. 10b, showing that the Airy and Flexural models coincide for low spherical harmonics degrees, and only mismatch for degrees higher than 30. However, the crustal thickness distribution presented in Figs. 8a and 9a differ, as the latter shows a smoother and more natural behaviour of the crust-mantle boundary for the Flexural model.

In order to further compare the crustal thickness variations provided by the three numerical models, Fig. 10a provides the crustal thickness based on each model along the 0.5° latitude line. Additionally, the topography is plotted to show its influence on the model. A few observations can be made: (1) the Airy and flexural models generally predict a thicker crust for higher topographies (as expected from hydrostatic equilibrium), and follow similar trends; (2) however, the Bouguer inversion occasionally predicts a thinner crust with positive topography (longitude $\approx 40^\circ$ and $\approx 150^\circ$, eg.), showing that it was not derived from a physical model and can lead to unexpected results. (3) while the Bouguer inversion and Flexural models provide a smooth crustal thickness variation, the Airy model is characterised by sharp spikes; (4) the flexural isostasy model resembles a moving average of the Airy model, resulting in a damping of the sharp spikes. Furthermore, comparing Figs. 7, 8, and 9 to Fig. 2, it can be noted that the flexural isostasy model is the most similar. On the one hand, the Airy isostasy model presents sharp local variations, whereas the results obtained by James, Zuber, and Phillips [14] are much smoother. On the other hand, the effects of the Beta, Phoebe, Themis, and Lada regions, which are all clearly visible in Fig. 2, are mostly absent from the Bouguer inversion results (although being present in the results from the flexural



(a) Crustal thickness based on the Airy isostasy model.

Figure 8: Airy isostasy numerical model results. The residuals map is saturated to the range -100 to 50 mGal, but has min=-170.8564 mGal, mean= 0.2973mGal, max=61.1463mGal, and std=23.0131mGal.



(a) Crustal thickness based on the flexural isostasy model.

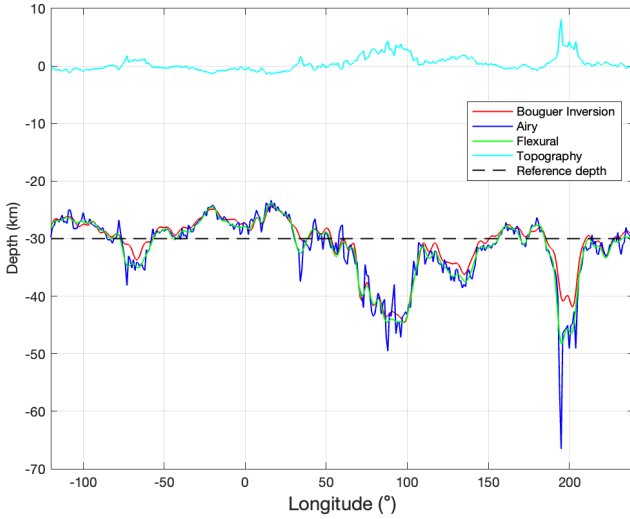
Figure 9: Flexural isostasy numerical model results. The residuals map is saturated to the range -100 to 50 mGal, but has min=-171.4694 mGal, mean=0.2997 mGal, max=60.7440 mGal, and std=23.0477 mGal.

isostasy model).

The different models can also be compared through their resulting gravity fields, as provided by the degree variance shown in Fig. 10b, from which a number of observations can be made: (1) the Bouguer inversion model and observations match exactly, which is expected from the derivation of the model aiming to reduce the gravity residuals to zero; (2) as already previously noted, the Airy and flexure models overlap at low spherical harmonic degree and start to differ for higher degrees, as expected from [20]; (3) the Airy and flexural models have consistently lower degree variance than the observed gravity field, which reveals that other components (such as density variations) have to be taken into account to better fit the observed data. As a result, the flexural isostasy model is found to be the most promising for subsequent work as it was derived from physics principles, does not overfit the data, shows a smooth behaviour of the crust-mantle boundary, and can be further optimised through its T_e parameter.

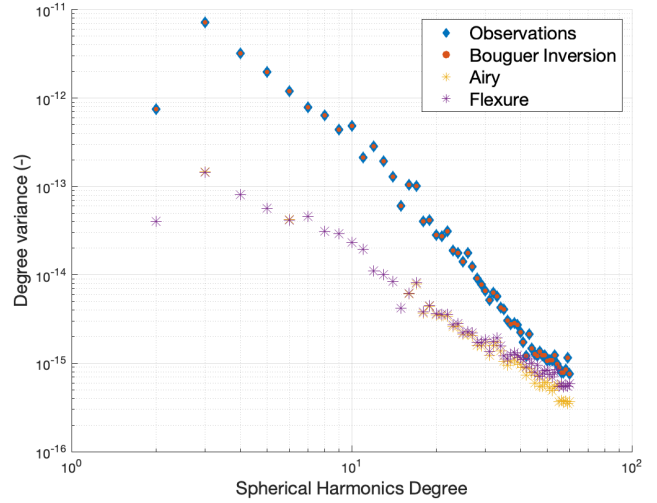
An improved fit of the degree variance of the flexural isostasy model is obtained using an optimal value of $T_e = 31.454\text{km}$ ($> 22\text{km}$ used originally), indicating that more flexure of the lithosphere than first anticipated is present. This fit shows a residual, Eq. (10), of 5.1553 (compared to 5.4711 for $T_e = 22\text{km}$). The value obtained is a bit higher than previously found by [24]. However, the gravity residuals of this model are still non-zero, which could be explained by lateral density variations across the crust. Those variations were determined through inversion of the gravity residuals, resulting in Fig. 11a, which shows densities ranging from 2753.2 to 2900.5 kg/m^3 . As the crust of Venus is believed to be majorly constituted of basalt [30], the range of densities obtained is realistic (basalt densities vary between 2700 and 3000 kg/m^3 [31]). No literature on the lateral density variations on the crust of Venus was found, meaning that those results could not be verified.

Those results can be compared to a simplified geological map of the planet from [27], as shown in Fig.



(a) Crustal thickness variation on the 0.5° latitude line for the Bouguer inversion, Airy isostasy, and flexural isostasy models.

Figure 10: Comparison between the different numerical models in terms of crustal thickness and degree variance of the gravity fields.



(b) Degree variance of the spherical harmonic gravity field from the observation data, Bouguer inversion, Airy isostasy, and flexural isostasy models.

11. From the comparison of Figs. 11a and 11b, it is clear that the lower density areas ($< 2840 \text{ kg/m}^3$) are associated to the tectonised terrains (Ishtar Terra and Aphrodite especially), which are also known to have a high topography from Fig. 4a. Global volcanic units, which have a lower topography, show a higher density ($> 2880 \text{ kg/m}^3$). However, little correlation is found between the “lifting related volcanism and tectonic components” and the density variations. Furthermore, impact craters and crater outflows features are generally smaller than the resolution of the derived density map, making any conclusions on the relation between those surface features and the density map impossible.

5 Approach Validity

The validity of the characterisation of the crust-mantle boundary depth through methods leveraging the isostasy principle has been questioned by Kirby [32], who shows a number of pitfalls in the use of isostatic gravity anomalies in general. Most notably, [32] notes that coexisting surface and subsurface loading cannot be faithfully represented with analytical isostasy models, and that most studies ignore the effects of the lithosphere flexural rigidity (modelled through the T_e parameter). As a result of those shortcomings of the method, the crust-mantle boundary depth can be over- or underestimated, and the size of the surface load which can be supported by the lithospheric plate without flexure is underestimated [32]. Therefore, the results obtained in this work should be considered as first to second order approximates of the true values only, and require further analysis and refinement.

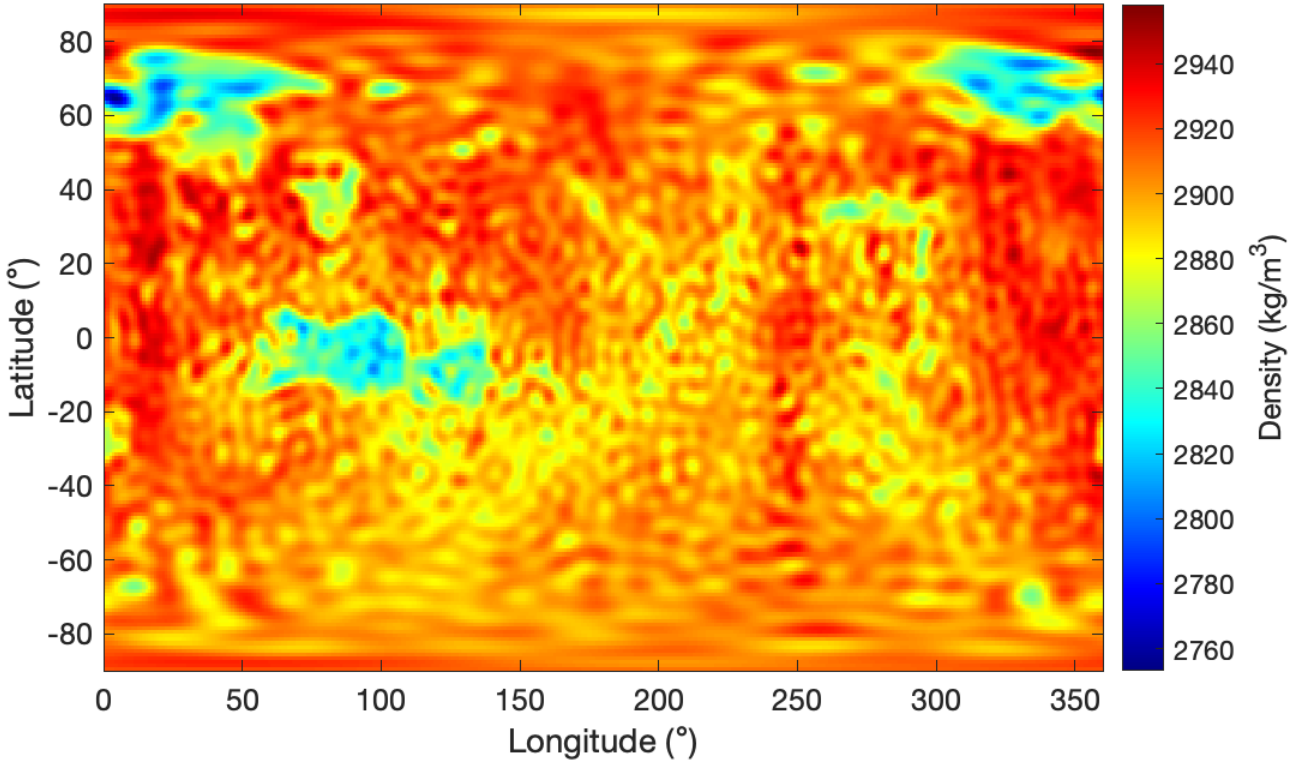
6 Conclusion

Three numerical models were developed to obtain the Venusian crustal thickness and density distributions across the planet. First, the Bouguer Inversion provided an overfit of the observation data and occasionally gave rise to unphysical values of the crustal thickness. Second, the Airy model was derived based on physical principles, but resulted in a very sharp peaks and fast changing behaviour of the crust-mantle boundary depth (local isostasy). Third, the flexural isostasy model (infinite plate bending) resulted in a smoother behaviour of the crustal thickness, while resulting similar gravity residuals to the Airy model. Comparison between the three models permitted to conclude that the flexural isostasy model has the most potential for further work.

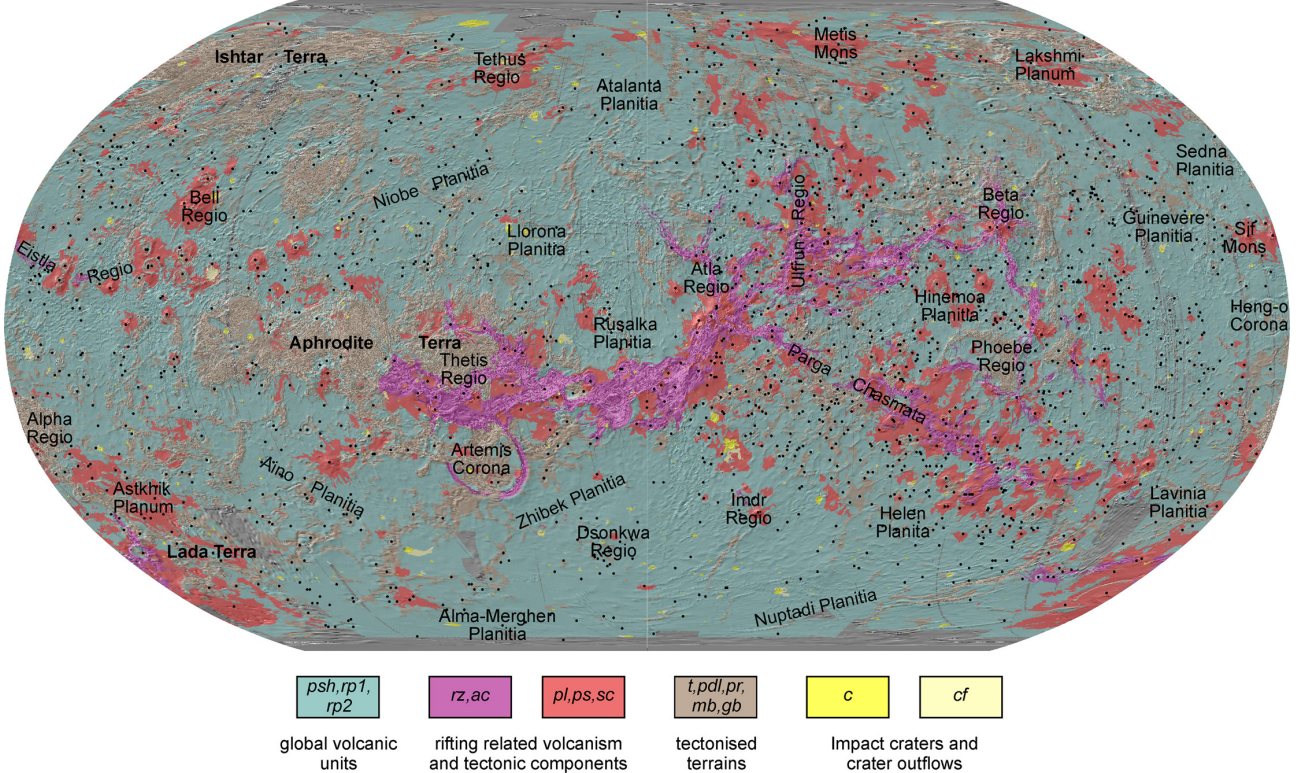
The optimal effective elastic thickness value, $T_e = 31.454 \text{ km}$, of the planet was determined by minimising the residual between the degree variance of the observed and modelled gravity fields. This optimal model was finally used to invert the lateral density variations in the crust. The latter permitted to conclude that the lower density regions to tectonised terrains in general.

Improvements on the developments and analysis performed in this work include:

1. The uncertainty in the results obtained, and the effects of the shortcomings mentioned in section 5 need to be quantified in order to build trust into the selected model.
2. Only the effects of crustal thickness and density variations were taken into account. However, density variations in the mantle, dynamical support and lithospheric stresses also have an impact on the structure of the lithosphere, and should be considered in refinements of the work presented.



(a) Lateral density variations in the crust obtained through inversion of the gravity residuals of the flexural isostasy crustal thickness model.



(b) Simplified geological map of Venus, modified after Platz *et al.* [26] by Platz *et al.* [27]. Following [27, p. 11]: “From that original source, the following units were merged to represent: (1) tectonized terrains – units t (tessera, Fortuna Formation), pdl (densely lineated plains, Atropos Formation), pr (ridged plains, Lavinia Formation), mb (mountain belts, Akna Formation) and gb (groove belts, Agrona Formation); (2) global volcanic terrains – units psh (shield plains, Accruva Formation), rp1 (regional plains 1, Rusalka Formation) and rp2 (regional plains 2, Ituana Formation); (3) rifting-related terrains – units pl (lobate plains, Bell Formation), ps (smooth plains, Gunda Formation) and sc (shield clusters, Boala Formation); and (4) tectonic components related to (3) – units rz (rift zones, Devana Formation) and ac (Artemis Canyon materials). Impact craters and crater outflows are shown as units c and cf, respectively. Individual tectonic structures are omitted for clarity. Black dots represent the locations of volcanic edifices Platz *et al.* [28]. Grey areas correspond to the radar-based hillshade (i.e. no mapping data available). The geological map is superimposed on a Magellan Global Topography Data Record shaded relief map (4.6 km/px) shown here in a Robinson projection, centred at 0°E.”.

Figure 11: Comparison between the lateral density variations derived from the optimised flexural isostasy model, and the simplified geological map from [27]. The density map was centred on the 180° longitude line to match the results of Platz *et al.* [27].

Bibliography

- [1] A. Aitta. "Venus' internal structure, temperature and core composition". In: *Icarus* 218.2 (2012), pp. 967–974. ISSN: 0019-1035. DOI: <https://doi.org/10.1016/j.icarus.2012.01.007>. URL: <https://www.sciencedirect.com/science/article/pii/S001910351200022X>.
- [2] T.L. Zhang *et al.* "Initial Venus Express magnetic field observations of the Venus bow shock location at solar minimum". In: *Planetary and Space Science* 56.6 (2008). Mars Express/Venus Express, pp. 785–789. ISSN: 0032-0633. DOI: <https://doi.org/10.1016/j.pss.2007.09.012>. URL: <https://www.sciencedirect.com/science/article/pii/S0032063307003777>.
- [3] *VIRTIS: The Visible and Infrared Thermal Imaging Spectrometer*. Vol. 1295. ESA Special Publication. Dec. 2007.
- [4] Robert R. Herrick and Roger J. Phillips. "Geological correlations with the interior density structure of Venus". In: *Journal of Geophysical Research: Planets* 97.E10 (1992), pp. 16017–16034. DOI: <https://doi.org/10.1029/92JE01498>. eprint: <https://agupubs.onlinelibrary.wiley.com/doi/pdf/10.1029/92JE01498>. URL: <https://agupubs.onlinelibrary.wiley.com/doi/abs/10.1029/92JE01498>.
- [5] V. N. Zharkov. "Models of the internal structure of Venus". In: *The moon and the planets* 29.2 (1983), pp. 139–175. DOI: [10.1007/BF00928322](https://doi.org/10.1007/BF00928322). URL: <https://doi.org/10.1007/BF00928322>.
- [6] V. N. Zharkov, T. V. Gudkova, and A. Nikol'skii. "On Parameters of the Earth-Like Model of Venus". In: *Solar System Research* 53.1 (2019), pp. 1–4. DOI: [10.1134/S0038094618060084](https://doi.org/10.1134/S0038094618060084). URL: <https://doi.org/10.1134/S0038094618060084>.
- [7] A.S. Konopliv, W.B. Banerdt, and W.L. Sjogren. "Venus Gravity: 180th Degree and Order Model". In: *Icarus* 139.1 (1999), pp. 3–18. ISSN: 0019-1035. DOI: <https://doi.org/10.1006/icar.1999.6086>. URL: <https://www.sciencedirect.com/science/article/pii/S0019103599960864>.
- [8] Agnes Fienga *et al.* "Exploring Venus internal structure and its tidal response". In: *EPSC-DPS Joint Meeting 2019*. Vol. 2019. Sept. 2019, EPSC-DPS2019-1939, EPSC-DPS2019-1939.
- [9] In: *Journal of Geophysical Research (1896-1977)* 75.17 (1970), pp. 3357–3365. DOI: <https://doi.org/10.1029/JB075i017p03357>. eprint: <https://agupubs.onlinelibrary.wiley.com/doi/pdf/10.1029/JB075i017p03357>. URL: <https://agupubs.onlinelibrary.wiley.com/doi/abs/10.1029/JB075i017p03357>.
- [10] Donald W. Forsyth. "Subsurface loading and estimates of the flexural rigidity of continental lithosphere". In: *Journal of Geophysical Research: Solid Earth* 90.B14 (1985), pp. 12623–12632. DOI: <https://doi.org/10.1029/JB090iB14p12623>. eprint: <https://agupubs.onlinelibrary.wiley.com/doi/pdf/10.1029/JB090iB14p12623>. URL: <https://agupubs.onlinelibrary.wiley.com/doi/abs/10.1029/JB090iB14p12623>.
- [11] Suzanne E. Smrekar. "Evidence for Active Hotspots on Venus from Analysis of Magellan Gravity Data". In: *Icarus* 112.1 (1994), pp. 2–26. ISSN: 0019-1035. DOI: <https://doi.org/10.1006/icar.1994.1166>. URL: <https://www.sciencedirect.com/science/article/pii/S0019103584711663>.
- [12] F. Scott Anderson and Suzanne E. Smrekar. "Global mapping of crustal and lithospheric thickness on Venus". In: *Journal of Geophysical Research: Planets* 111.E8 (2006). DOI: <https://doi.org/10.1029/2004JE002395>. eprint: <https://agupubs.onlinelibrary.wiley.com/doi/pdf/10.1029/2004JE002395>. URL: <https://agupubs.onlinelibrary.wiley.com/doi/abs/10.1029/2004JE002395>.
- [13] DaiYun Wei, An Yang, and JinShui Huang. "The gravity field and crustal thickness of Venus". In: *Science China Earth Sciences* 57.9 (2014), pp. 2025–2035. DOI: [10.1007/s11430-014-4824-5](https://doi.org/10.1007/s11430-014-4824-5). URL: <https://doi.org/10.1007/s11430-014-4824-5>.
- [14] Peter B. James, Maria T. Zuber, and Roger J. Phillips. "Crustal thickness and support of topography on Venus". In: *Journal of Geophysical Research: Planets* 118.4 (2013), pp. 859–875. DOI: <https://doi.org/10.1029/2012JE004237>. eprint: <https://agupubs.onlinelibrary.wiley.com/doi/pdf/10.1029/2012JE004237>. URL: <https://agupubs.onlinelibrary.wiley.com/doi/abs/10.1029/2012JE004237>.
- [15] Jinshui Huang, An Yang, and Shijie Zhong. "Constraints of the topography, gravity and volcanism on Venusian mantle dynamics and generation of plate tectonics". In: *Earth and Planetary Science Letters* 362 (2013), pp. 207–214. ISSN: 0012-821X. DOI: <https://doi.org/10.1016/j.epsl.2012.11.051>. URL: <https://www.sciencedirect.com/science/article/pii/S0012821X12006772>.
- [16] R. L. Parker. "The Rapid Calculation of Potential Anomalies". In: *Geophysical Journal International* 31.4 (Mar. 1973), pp. 447–455. ISSN: 0956-540X. DOI: [10.1111/j.1365-246X.1973.tb06513.x](https://doi.org/10.1111/j.1365-246X.1973.tb06513.x). eprint: <https://academic.oup.com/gji/article-pdf/31/4/447/1603529/31-4-447.pdf>. URL: <https://doi.org/10.1111/j.1365-246X.1973.tb06513.x>.
- [17] NASA PDS. *Magellan Spherical Harmonics, Topography, and Gravity Data*. 2023. URL: https://pds-geosciences.wustl.edu/missions/magellan/shadr_topo_grav/index.htm.

- [18] Peter G. Ford and Gordon H. Pettengill. “Venus topography and kilometer-scale slopes”. In: *Journal of Geophysical Research: Planets* 97.E8 (1992), pp. 13103–13114. DOI: <https://doi.org/10.1029/92JE01085>. eprint: <https://agupubs.onlinelibrary.wiley.com/doi/pdf/10.1029/92JE01085>. URL: <https://agupubs.onlinelibrary.wiley.com/doi/abs/10.1029/92JE01085>.
- [19] B. C. Root. *GSH is a MATLAB package to do Global Spherical Harmonic Analyses (GSHA) and Synthesis (GSHS) for Crust1.0*. Version 1. [Computer software]. 2021. URL: <https://doi.org/10.4121/16764238.V1>.
- [20] A. B. Watts and J. D. P. Moore. “Flexural Isostasy: Constraints From Gravity and Topography Power Spectra”. In: *Journal of Geophysical Research: Solid Earth* 122.10 (2017), pp. 8417–8430. DOI: <https://doi.org/10.1002/2017JB014571>. eprint: <https://agupubs.onlinelibrary.wiley.com/doi/pdf/10.1002/2017JB014571>. URL: <https://agupubs.onlinelibrary.wiley.com/doi/abs/10.1002/2017JB014571>.
- [21] Weikko Aleksanteri Heiskanen and Felix Andries Vening Meinesz. *The earth and its gravity field*. McGraw-Hill, 1958.
- [22] MatWeb. *Basalt*. 2023. URL: <https://www.matweb.com/search/datasheet.aspx?matguid=9642fc0c676740659233201627b67b73&ckck=1>.
- [23] Benedek A. Lógó and Balazs Vasarhelyi. “Estimation of the Poisson’s Rate of the Intact Rock in the Function of the Rigidity”. In: *Periodica Polytechnica Civil Engineering* (Oct. 2019). DOI: [10.3311/PPci.14946](https://doi.org/10.3311/PPci.14946).
- [24] David N. Barnett, Francis Nimmo, and Dan McKenzie. “Elastic Thickness Estimates for Venus Using Line of Sight Accelerations from Magellan Cycle 5”. In: *Icarus* 146.2 (2000), pp. 404–419. ISSN: 0019-1035. DOI: <https://doi.org/10.1006/icar.2000.6352>. URL: <https://www.sciencedirect.com/science/article/pii/S0019103500963528>.
- [25] Peter B. James, Maria T. Zuber, and Roger J. Phillips. “Crustal thickness and support of topography on Venus”. In: *Journal of Geophysical Research: Planets* 118.4 (2013), pp. 859–875. DOI: <https://doi.org/10.1029/2012JE004237>. eprint: <https://agupubs.onlinelibrary.wiley.com/doi/pdf/10.1029/2012JE004237>. URL: <https://agupubs.onlinelibrary.wiley.com/doi/abs/10.1029/2012JE004237>.
- [26] T. Platz *et al.* “Volcanism and tectonism across the inner solar system: an overview”. In: *Geological Society, London, Special Publications* 401.1 (2015), pp. 1–56. DOI: [10.1144/SP401.22](https://doi.org/10.1144/SP401.22). eprint: <https://www.lyellcollection.org/doi/pdf/10.1144/SP401.22>. URL: <https://www.lyellcollection.org/doi/abs/10.1144/SP401.22>.
- [27] T. Platz *et al.* “Volcanism and tectonism across the inner solar system: an overview”. In: *Geological Society, London, Special Publications* 401.1 (2015), pp. 1–56. DOI: [10.1144/SP401.22](https://doi.org/10.1144/SP401.22). eprint: <https://www.lyellcollection.org/doi/pdf/10.1144/SP401.22>. URL: <https://www.lyellcollection.org/doi/abs/10.1144/SP401.22>.
- [28] T. Platz *et al.* “Volcanism and tectonism across the inner solar system: an overview”. In: *Geological Society, London, Special Publications* 401.1 (2015), pp. 1–56. DOI: [10.1144/SP401.22](https://doi.org/10.1144/SP401.22). eprint: <https://www.lyellcollection.org/doi/pdf/10.1144/SP401.22>. URL: <https://www.lyellcollection.org/doi/abs/10.1144/SP401.22>.
- [29] Robert Tenzer *et al.* “How to Calculate Bouguer Gravity Data in Planetary Studies”. In: *Surveys in Geophysics* 40.1 (2019), pp. 107–132. DOI: [10.1007/s10712-018-9504-0](https://doi.org/10.1007/s10712-018-9504-0). URL: <https://doi.org/10.1007/s10712-018-9504-0>.
- [30] Suzanne E. Smrekar, Anne Davaille, and Christophe Sotin. “Venus Interior Structure and Dynamics”. In: *Space Science Reviews* 214.5 (2018), p. 88. DOI: [10.1007/s11214-018-0518-1](https://doi.org/10.1007/s11214-018-0518-1). URL: <https://doi.org/10.1007/s11214-018-0518-1>.
- [31] James G Moore. “Density of basalt core from Hilo drill hole, Hawaii”. In: *Journal of Volcanology and Geothermal Research* 112.1 (2001), pp. 221–230. ISSN: 0377-0273. DOI: [https://doi.org/10.1016/S0377-0273\(01\)00242-6](https://doi.org/10.1016/S0377-0273(01)00242-6). URL: <https://www.sciencedirect.com/science/article/pii/S0377027301002426>.
- [32] Jon F Kirby. “On the pitfalls of Airy isostasy and the isostatic gravity anomaly in general”. In: *Geophysical Journal International* 216.1 (Oct. 2018), pp. 103–122. ISSN: 0956-540X. DOI: [10.1093/gji/ggy411](https://doi.org/10.1093/gji/ggy411). eprint: <https://academic.oup.com/gji/article-pdf/216/1/103/26257783/ggy411.pdf>. URL: <https://doi.org/10.1093/gji/ggy411>.

A MATLAB Code

The entirety of the code used in this assignment was attached in the form of a zip file to the Brightspace submission.